Applications of Mathematics

Wonho Han; Kwangil Kim; Unhyok Hong Convergence of a proposed adaptive WENO scheme for Hamilton-Jacobi equations

Applications of Mathematics, Vol. 68 (2023), No. 5, 661-684

Persistent URL: http://dml.cz/dmlcz/151838

Terms of use:

© Institute of Mathematics AS CR, 2023

Institute of Mathematics of the Czech Academy of Sciences provides access to digitized documents strictly for personal use. Each copy of any part of this document must contain these *Terms of use*.



This document has been digitized, optimized for electronic delivery and stamped with digital signature within the project *DML-CZ*: *The Czech Digital Mathematics Library* http://dml.cz

CONVERGENCE OF A PROPOSED ADAPTIVE WENO SCHEME FOR HAMILTON-JACOBI EQUATIONS

Wonho Han, Kwangil Kim, Unhyok Hong, Pyongyang

Received November 12, 2022. Published online August 9, 2023.

Abstract. We study high-order numerical methods for solving Hamilton-Jacobi equations. Firstly, by introducing new clear concise nonlinear weights and improving their convex combination, we develop WENO schemes of Zhu and Qiu (2017). Secondly, we give an algorithm of constructing a convergent adaptive WENO scheme by applying the simple adaptive step on the proposed WENO scheme, which is based on the introduction of a new singularity indicator. Through detailed numerical experiments on extensive problems including nonconvex ones, the convergence and effectiveness of the adaptive WENO scheme are demonstrated.

Keywords: Hamilton-Jacobi equations; WENO scheme; adaptive WENO scheme; nonconvex Hamiltonian; convergence

MSC 2020: 35F21, 65M12, 65M06

1. Introduction

In this paper, we study numerical methods of solving the Hamilton-Jacobi (H-J) equation

(1.1)
$$\begin{cases} \varphi_t + H(x, t, \varphi, \nabla \varphi) = 0, & (x, t) \in \mathbb{R}^d \times (0, T], \\ \varphi(x, 0) = \varphi_0(x), & x \in \mathbb{R}^d. \end{cases}$$

The first-order monotone scheme by Crandal and Lions [6] is an important class of numerical methods for H-J equations. The monotone scheme converges to the viscosity solution but has at most first-order accuracy. Therefore, the convergence rate is relatively low and the acute parts which express the main feature of the solution become heavily smeared.

In the last two decades, more accurate numerical methods for Hamilton-Jacobi equations have been extensively studied. Weighted essentially nonoscillatory schemes

DOI: 10.21136/AM.2023.0264-22

(WENO for short) are most widely used high-order numerical methods applied to convection dominated problems as well as H-J equations [10], [11], [16], [18], [21]. By using adaptive stencils and a weighted convex combination in the reconstruction process of the derivative, WENO schemes achieve high-order accuracy in smooth regions and give not only essentially nonoscillatory but also sharp approximations near singularities. The fifth-order finite difference WENO scheme for H-J equations initially proposed in [10] was generalized to unstructured meshes [23] and developed to several variants [8], [21], [22], [2]. We also refer to central WENO schemes [4], [15], which consist of applications of the discrete projection and the exact evolution, and Hermite WENO schemes [20], [24], which use not only the function but also its first derivative in the WENO reconstruction and therefore possess the compactness. In [9], the author developed a WENO scheme by introducing a new family of smoothness indicators. In the above-mentioned classical WENO schemes, the fifth-order WENO reconstruction of the derivative is performed by the convex combination of three third-order approximations.

Recently, Zhu and Qiu [25], [26] proposed a WENO scheme which uses the convex combination of a fifth-order approximation and two second-order ones in the WENO reconstruction of the first derivative. This new WENO scheme, which uses the same number of spatial nodes and could get less absolute truncation errors, sustains superior numerical properties of traditional WENO schemes, such as high-order accuracy, nonoscillatory work behavior and so on. We notice here that the meaning of linear weights in the WENO scheme of Zhu and Qiu [26] is different from the ones in classical WENO schemes which are uniquely defined to achieve the fifthorder approximation of derivative through linearly combining with the third-order approximations. In fact, the linear weights in [26] may be taken as any positive and merely act as a sort of parameters which affect WENO reconstruction of derivative. Therefore, we regard that there is no necessity to think about the artificial linear weights as in [26]. Moreover, the meaning of nonlinear weights defined in [26] is not very clear and as a result, the nonlinear combination in the WENO reconstruction also becomes complicated. From such standpoint, we try to find new clear concise variants of the nonlinear weights and improve the tedious convex combination in [26], which is the subject of Section 2.

On the other hand, despite of remarkable properties of the high-order numerical methods, theoretical results on their convergence are rarely known for H-J equations [5], [21]. As one knows, pure WENO schemes are difficult to expect the convergence for special cases of nonconvex problems. In general, the behavior of viscosity solution of a local Riemann problem near a singular point depends highly on convexness-concaveness of the Hamiltonian, and according to the problem, new singularities in the solution may develop in different aspects as time elapses. High-

order schemes, which are based on more compressive reconstruction of derivative as compared to the first-order schemes, occasionally fail to capture such appearances of new singularities.

The study of convergent high-order numerical methods has been mainly performed in the direction of combining a high-order scheme with a lower (first) order one [1], [14]. Adaptive algorithms in [13], [12], [19] and filtered schemes in [3], [17] are all based on the former-mentioned methodology. The common merits peculiar to all such schemes are that they all converge and still inherit numerical properties from high-order schemes, such as high-order accuracy and good singularity resolution. Therefore, one must properly modify the WENO scheme to achieve the high-order accurate numerical approximation and assure the convergence at the same time, and we propose a simple adaptive algorithm for that in Section 3.

This paper is organized as follows. In Section 2, we newly define a sort of clear concise nonlinear weights during the WENO reconstruction in such way as [26] and then propose an improved WENO scheme. Section 3 proposes an algorithm of constructing a convergent adaptive WENO scheme by adapting the proposed WENO scheme through a newly introduced singularity indicator. Detailed numerical experiments are performed to show the ability of proposed schemes in Section 4. Concluding remarks are given in Section 5.

2. An improved WENO scheme

In this section, we develop the WENO scheme of Zhu and Qiu [26] by introducing new nonlinear weights and improving convex combination for WENO reconstruction.

2.1. WENO scheme for the one-dimensional case. Consider the one-dimensional model problem of Hamilton-Jacobi equation

(2.1)
$$\begin{cases} \varphi_t + H(\varphi_x) = 0, & (x,t) \in \mathbb{R} \times (0,T], \\ \varphi(x,0) = \varphi_0(x), & x \in \mathbb{R}. \end{cases}$$

We divide the real line \mathbb{R} into uniform mesh with equal spacing h > 0 and denote the mesh points by $x_i = ih$, $i \in \mathbb{Z}$. We also put $\varphi_i = \varphi(x_i, t)$, $D^{\pm}\varphi_i = \pm(\varphi_{i\pm 1} - \varphi_i)/h$. The semi-discrete scheme for the equation (2.1) is defined by

(2.2)
$$\frac{\mathrm{d}\varphi_i(t)}{\mathrm{d}t} = -\widetilde{H}(\varphi_{x,i}^-, \varphi_{x,i}^+), \quad i \in \mathbb{Z},$$

where \widetilde{H} is a Lipschitz continuous monotone flux consistent with H and $\varphi_{x,i}^{\pm}$ are approximations of the first derivative from the left and right sides of the point x_i .

There may be different schemes according to the method of determining $\varphi_{x,i}^{\pm}$ at x_i , and we follow the procedure in [26] for WENO reconstruction here. The procedure of WENO reconstruction is as follows.

Step 1: Approximations of the derivative by interpolation polynomials. We denote by $p_l^-(x)$, l=1,2,3, the derivatives of a fifth degree polynomial and two quadratic polynomials defined on left-biased point stencils $\{x_{i-3},\ldots,x_{i+2}\}$, $\{x_{i-2},x_{i-1},x_i\}$ and $\{x_{i-1},x_i,x_{i+1}\}$, respectively. Then $\varphi_{x,i}^{-,l}:=p_l^-(x_i)$, l=1,2,3, the fifth and second-order approximations of $\varphi_x(x_i)$ are explicitly defined as (see [26])

$$(2.3) \quad \varphi_{x,i}^{-,1} = \frac{1}{30} D^+ \varphi_{i-3} - \frac{13}{60} D^+ \varphi_{i-2} + \frac{47}{60} D^+ \varphi_{i-1} + \frac{9}{20} D^+ \varphi_i - \frac{1}{20} D^+ \varphi_{i+1},$$

(2.4)
$$\varphi_{x,i}^{-,2} = -\frac{1}{2}D^+\varphi_{i-2} + \frac{3}{2}D^+\varphi_{i-1},$$

(2.5)
$$\varphi_{x,i}^{-,3} = \frac{1}{2}D^+\varphi_{i-1} + \frac{1}{2}D^+\varphi_i.$$

We also denote by $p_l^+(x)$, l=1,2,3, the derivatives of three approximation polynomials defined on right-biased point stencils $\{x_{i-2},\ldots,x_{i+3}\}$, $\{x_{i-1},x_i,x_{i+1}\}$ and $\{x_i,x_{i+1},x_{i+2}\}$, respectively, and obtain $\varphi_{x,i}^{+,l}$, l=1,2,3, the values of $p_l^+(x)$, l=1,2,3, at the point x_i .

Step 2: Computation of smoothness indicators β_l^{\pm} , l=1,2,3. The smoothness indicators β_l^{-} , l=1,2,3, are the quantitative estimators which measure how smooth the functions $p_l^{-}(x)$, l=1,2,3, are in interval $[x_{i-1},x_i]$. We use the same definition of smoothness indicators as in [11] here.

(2.6)
$$\beta_l^- = \sum_{k=1}^{r_l} \int_{x_{i-1}}^{x_i} h^{2k-1} \left(\frac{\mathrm{d}^k p_l^-}{\mathrm{d} x^k}\right)^2 \mathrm{d} x, \quad l = 1, 2, 3,$$

where $r_1 = 4$ and $r_2 = r_3 = 1$.

The smoothness indicators β_l^+ , l = 1, 2, 3, which measure how smooth the functions are in the interval $[x_i, x_{i+1}]$, are defined similarly.

Expanding in Taylor series, the following expressions are obtained.

(2.7)
$$\beta_1^- = h^2(\varphi_i'')^2 - h^3 \varphi_i'' \cdot \varphi_i^{(3)} + O(h^4),$$

(2.8)
$$\beta_2^- = h^2(\varphi_i'')^2 - 2h^3\varphi_i'' \cdot \varphi_i^{(3)} + O(h^4),$$

(2.9)
$$\beta_3^- = h^2(\varphi_i'')^2 + \frac{h^4}{6}\varphi_i'' \cdot \varphi_i^{(4)} + O(h^6),$$

(2.10)
$$\beta_1^+ = h^2(\varphi_i'')^2 + h^3 \varphi_i'' \cdot \varphi_i^{(3)} + O(h^4),$$

(2.11)
$$\beta_2^+ = h^2(\varphi_i'')^2 + \frac{h^4}{6}\varphi_i'' \cdot \varphi_i^{(4)} + O(h^6),$$

(2.12)
$$\beta_3^+ = h^2(\varphi_i'')^2 + 2h^3\varphi_i'' \cdot \varphi_i^{(3)} + O(h^4).$$

Step 3: Definition of new nonlinear weights. We first introduce the quantity

(2.13)
$$\tau^{\pm} = \max\{|\beta_1^{\pm} - \beta_2^{\pm}|^2, |\beta_1^{\pm} - \beta_3^{\pm}|^2\}.$$

Nonlinear weights ω_l^{\pm} , l=1,2,3, used in combining $\varphi_{x,i}^{\pm,l}$, l=1,2,3, are defined by

(2.14)
$$\omega_l^{\pm} = \frac{\overline{\omega}_l^{\pm}}{\sum_{j=1}^3 \overline{\omega}_j^{\pm}}, \quad l = 1, 2, 3,$$

where

(2.15)
$$\overline{\omega}_1^{\pm} = \nu_1 \left(1 + \frac{\tau^{\pm}}{\varepsilon + \beta_1^{\pm}} \right), \quad \overline{\omega}_2^{\pm} = \frac{\nu_2 \tau^{\pm}}{\varepsilon + \beta_2^{\pm}}, \quad \overline{\omega}_3^{\pm} = \frac{\nu_3 \tau^{\pm}}{\varepsilon + \beta_3^{\pm}}$$

and the three parameters ν_l , l=1,2,3, are positive numbers which are properly selected (their sum is not necessarily equal to 1). Here ε is used to avoid the denominator from becoming zero and taken as $\varepsilon \approx 10^{-6}$ in computational practice.

Step 4: WENO reconstructions of $\varphi_x(x_i)$. The WENO reconstructions $\varphi_{x,i}^{\pm}$ are defined by

(2.16)
$$\varphi_{x,i}^{\pm} = \omega_1^{\pm} \varphi_{x,i}^{\pm,1} + \omega_2^{\pm} \varphi_{x,i}^{\pm,2} + \omega_3^{\pm} \varphi_{x,i}^{\pm,3}.$$

Now, we proceed with some discussions on WENO reconstructions. Considering (2.7) to (2.12) and (2.13), it is immediate to verify in smooth regions of the numerical solution

(2.17)
$$\frac{\tau^{\pm}}{\varepsilon + \beta_{l}^{\pm}} = O(h^{4}), \quad l = 1, 2, 3,$$

on the condition that $\varepsilon \ll \beta_l^{\pm}$, l=1,2,3. Therefore, we get $\omega_2^{\pm} = O(h^4)$, $\omega_3^{\pm} = O(h^4)$ in smooth regions of the solution, and after all,

$$\varphi_{x,i}^{\pm} = \omega_1^{\pm}(\varphi_x(x_i) + O(h^5)) + \omega_2^{\pm}(\varphi_x(x_i) + O(h^2)) + \omega_3^{\pm}(\varphi_x(x_i) + O(h^2))$$
$$= (\omega_1^{\pm} + \omega_2^{\pm} + \omega_3^{\pm})\varphi_x(x_i) + O(h^5) = \varphi_x(x_i) + O(h^5),$$

providing the formal fifth-order accuracy of the WENO reconstruction.

On the other hand, we assume that the solution is rough on the big spatial stencil (thus, discontinuity in the solution derivative appears near the target point). As a result, if $\beta_2^- \ll \beta_1^-$ and $\beta_3^- \ll \beta_1^-$ ($\beta_2^+ \ll \beta_1^+$ and $\beta_3^+ \ll \beta_1^+$), we get from (2.13)

$$\beta_2^\pm \ll \tau^\pm, \quad \beta_3^\pm \ll \tau^\pm \quad \text{and} \quad \tau^\pm/\beta_1^\pm = O(1).$$

Therefore, the following estimations hold from the definition of nonlinear weights:

$$\omega_2^- \gg \omega_1^- \quad \text{and} \quad \omega_3^- \gg \omega_1^- \quad (\omega_2^+ \gg \omega_1^+ \text{ and } \omega_3^+ \gg \omega_1^+).$$

Then two second-order approximations are used in the WENO reconstruction, which are evaluated from two smaller three-point stencils, where the solution is smooth.

Especially, if $\beta_2^-\ll\beta_1^-$ and $\beta_2^-\ll\beta_3^-$ ($\beta_3^-\ll\beta_1^-$ and $\beta_3^-\ll\beta_2^-$), we get

$$\beta_2^- \ll \tau^-, \quad \tau^-/\beta_1^- = O(1) \quad \text{and} \quad \tau^-/\beta_3^- = O(1)$$

 $(\beta_3^- \ll \tau^-, \ \tau^-/\beta_1^- = O(1) \text{ and } \tau^-/\beta_2^- = O(1)).$

Therefore, $\omega_2^- \gg \omega_1^-$ and $\omega_2^- \gg \omega_3^-$ ($\omega_3^- \gg \omega_1^-$ and $\omega_3^- \gg \omega_2^-$), and then the second-order approximations $\varphi_{x,i}^{-,2}(\varphi_{x,i}^{-,3})$ are used in WENO reconstruction, which is evaluated from the stencils $\{x_{i-2},x_{i-1},x_i\}$ ($\{x_{i-1},x_i,x_{i+1}\}$), where the solution is locally smooth. Similar facts also hold in case that $\beta_2^+ \ll \beta_1^+$ and $\beta_2^+ \ll \beta_3^+$ ($\beta_3^+ \ll \beta_1^+$ and $\beta_3^+ \ll \beta_2^+$).

After all, the WENO reconstructions (2.16) possess both necessary numerical properties, thus the high (fifth) order accuracy in smooth regions of the solution and numerical stability (nonoscillating property) near singular points.

Remark 2.1. In comparison with (2.16), WENO approximation in [26] could be rewritten as

$$(2.18) \qquad \varphi_{x,i}^{\pm} = \frac{1}{\overline{\omega}^{\pm}} \left(1 + \frac{\tau^{\pm}}{\varepsilon + \beta_{1}^{\pm}} \right), \quad l = 1, 2, 3,$$

$$(2.18) \qquad \varphi_{x,i}^{\pm} = \frac{1}{\overline{\omega}^{\pm}} \left(1 + \frac{\tau^{\pm}}{\varepsilon + \beta_{1}^{\pm}} \right) \varphi_{x,i}^{\pm, 1} + \frac{\nu_{2}}{\overline{\omega}^{\pm}} \left(\frac{\tau^{\pm}}{\varepsilon + \beta_{2}^{\pm}} - \frac{\tau^{\pm}}{\varepsilon + \beta_{1}^{\pm}} \right) \varphi_{x,i}^{\pm, 2} + \frac{\nu_{3}}{\overline{\omega}^{\pm}} \left(\frac{\tau^{\pm}}{\varepsilon + \beta_{3}^{\pm}} - \frac{\tau^{\pm}}{\varepsilon + \beta_{1}^{\pm}} \right) \varphi_{x,i}^{\pm, 3}, \quad \overline{\omega}^{\pm} = \overline{\omega}_{1}^{\pm} + \overline{\omega}_{2}^{\pm} + \overline{\omega}_{3}^{\pm}.$$

In contrast to (2.18), we have defined new nonlinear weights and improved convex combination in the WENO reconstruction, which are not only simpler but also have clearer meaning than the previous ones. Here, we emphasize that ν_l , l = 1, 2, 3, are not the linear weights in meaning, but parameters which are properly selected according to the problems (their sum is not necessarily equal to 1).

The semi-discrete scheme (2.2) is rewritten as the ODE

(2.19)
$$\frac{\mathrm{d}\varphi_i(t)}{\mathrm{d}t} = L_i(\varphi), \quad i \in \mathbb{Z},$$

where L_i is a Lipschitz continuous numerical flux defined by the right-hand side in (2.2).

Let $\Delta t > 0$ be a time step and $\Delta t = T/N$ for some $N \ge 1$. A uniform mesh in time is defined by $t_n := n\Delta t$, $n \in \{0, ..., N\}$. Then we use the third-order TVD Runge-Kutta discretization method [7],

(2.20)
$$\begin{cases} \varphi_i^{(1)} = \varphi_i^n + \Delta t L_i(\varphi^n), \\ \varphi_i^{(2)} = \frac{3}{4} \varphi_i^n + \frac{1}{4} \varphi_i^{(1)} + \frac{1}{4} \Delta t L_i(\varphi^{(1)}), \\ \varphi_i^{n+1} = \frac{1}{3} \varphi_i^n + \frac{2}{3} \varphi_i^{(2)} + \frac{2}{3} \Delta t L_i(\varphi^{(2)}), \end{cases}$$

to obtain the fully discrete WENO scheme.

2.2. Two-dimensional case. WENO schemes for two-dimensional problems are directly obtained from the one-dimensional method.

We take the two-dimensional H-J equation

(2.21)
$$\begin{cases} \varphi_t + H(\varphi_x, \varphi_y) = 0, & (x, y, t) \in \mathbb{R}^2 \times (0, T], \\ \varphi(x, y, 0) = \varphi_0(x, y), & (x, y) \in \mathbb{R}^2. \end{cases}$$

For simplicity, we divide the space \mathbb{R}^2 into uniform mesh and denote by $\varphi_{i,j}$ the approximation of solution φ at the mesh point (x_i, y_j) . The semi-discrete scheme for the equation (2.21) is

(2.22)
$$\frac{\mathrm{d}\varphi_{i,j}(t)}{\mathrm{d}t} = -\widetilde{H}(\varphi_{x,i,j}^-, \varphi_{x,i,j}^+, \varphi_{y,i,j}^-, \varphi_{y,i,j}^+),$$

where \widetilde{H} is a Lipschitz continuous monotone flux consistent with H and $\varphi_{x,i,j}^{\pm}, \varphi_{y,i,j}^{\pm}$ are WENO approximations of partial derivatives at the point (x_i, y_j) , respectively. Then by using a dimension-by-dimension method, $\varphi_{x,i,j}^{\pm}$ and $\varphi_{y,i,j}^{\pm}$ are directly obtained from the one-dimensional case with fixed subscripts j or i, respectively.

3. Adaptive WENO scheme

In general, the convergence of WENO schemes for H-J equations could not be expected, including nonconvex problems with Lipschitz continuous initial conditions [13]. Here, we give an adaptive algorithm of constructing a convergent high-order scheme by modifying the WENO scheme proposed in Section 2.

The point at the issue of constructing a convergent adaptive scheme of WENO type is how to determine approximations of the derivative $\varphi_{x,i}^{\pm}$ at every mesh point x_i . Below, we denote by $\varphi_{i,A}^{-}(\varphi_{i,A}^{+})$ the WENO approximation of the left (right) derivative at the point x_i and by $\varphi_{i,M}^{-}(\varphi_{i,M}^{+})$ the first-order approximation, respectively.

First of all, it is natural to use as high-order approximations of the derivative as possible from the demand on high-order accuracy of the adaptive scheme. If the solution is smooth near the point x_i , the WENO approximation of the derivative is high-order accurate. Especially, if the solution is smooth in the local region including the left-biased three-point stencil $\{x_{i-2}, x_{i-1}, x_i\}$ or $\{x_{i-1}, x_i, x_{i+1}\}$, the WENO approximation $\varphi_{i,A}^-$ has still high-order (at least second order) accuracy (when the large six-point stencil may be inoperative). Similarly, if the solution is smooth on the right-biased three-point stencil $\{x_{i-1}, x_i, x_{i+1}\}$ or $\{x_i, x_{i+1}, x_{i+2}\}$, the WENO approximation $\varphi_{i,A}^+$ has also high-order (at least second order) accuracy. Therefore, we could approximate the derivative $\varphi_x(x_i)$ by using the WENO approximations $\varphi_{i,A}^+$ in these cases. In other cases, we use the first-order approximations instead of WENO approximations from the demand on the convergence of the adaptive scheme to be constructed.

In order to reflect these demands into the adaptive scheme, we firstly introduce a singularity indicator, which measures the local singularity of the numerical solution at the left (right) neighborhood of the point x_i ,

(3.1)
$$\beta_0^- = \min\{\beta_2^-, \beta_3^-\} \quad (\beta_0^+ = \min\{\beta_2^+, \beta_3^+\}),$$

where β_2^{\pm} and β_3^{\pm} are the smoothness indicators defined in Section 2, respectively.

We could know from relation (3.1) that if the solution is smooth in the interval $(x_{i-1}, x_i)((x_i, x_{i+1}))$, the left (right) neighborhood of the point x_i , then $\beta_0^-(\beta_0^+) = O(h^2)$ and in other cases (when the singularity appears), $\beta_0^-(\beta_0^+) = O(1)$.

Then we take the proper positive number (threshold) $\delta(\approx O(h))$ and, based on the estimation on the singularity indicator β_0^{\pm} , define the adaptive approximations of the derivative at the point x_i by

(3.2)
$$\varphi_{x,i}^{\pm} = \begin{cases} \varphi_{i,A}^{\pm} & \text{if } \beta_0^{\pm} < \delta, \\ \varphi_{i,M}^{\pm} & \text{otherwise.} \end{cases}$$

The algorithm for convergent adaptive scheme of the WENO type follows.

Algorithm 1 (Adaptive WENO scheme: one-dimensional case).

- (i) Perform the WENO reconstructions $\varphi_{i,A}^{\pm}$ of derivative at the point x_i .
- (ii) Compute the singularity indicator β_0^{\pm} according to (3.1).
- (iii) Determine adaptive approximations of the derivative. After taking a threshold δ , define the adaptive approximations of the derivative at x_i according to (3.2).
- (iv) Using the third-order TVD Runge-Kutta time discretization method, construct the full discrete adaptive WENO scheme.

Algorithm 1 is directly extended to the two-dimensional case. The singularity indicators at the point (x_i, y_j) are defined by

(3.3)
$$\beta_{x,0}^{\pm} = \min\{\beta_{x,2}^{\pm}, \beta_{x,3}^{\pm}\}, \quad \beta_{y,0}^{\pm} = \min\{\beta_{y,2}^{\pm}, \beta_{y,3}^{\pm}\},$$

where $\beta_{x,2}^{\pm}$ and $\beta_{x,3}^{\pm}$ are the smoothness indicators defined from the one-dimensional case with a fixed subscript j ($\beta_{y,2}^{\pm}$ and $\beta_{y,3}^{\pm}$ are similarly defined with a fixed subscript i). Then using a properly selected positive number (threshold) $\delta(\approx O(h))$, we define adaptive approximations of the partial derivative φ_x at the point (x_i, y_j) by

(3.4)
$$\varphi_{x,i,j}^{\pm} = \begin{cases} \varphi_{x,i,j}^{\pm,M} & \text{if } \beta_{x,0}^{\pm} < \delta, \\ \varphi_{x,i,j}^{\pm,M} & \text{otherwise,} \end{cases}$$

where $\varphi_{x,i,j}^{\pm,A}$ ($\varphi_{x,i,j}^{\pm,M}$) are the WENO (first order) approximations of the partial derivative φ_x at the point (x_i, y_j) . The adaptive approximations of φ_y are determined similarly.

Algorithm 2 (Adaptive WENO scheme: two-dimensional case).

- (i) Perform the WENO reconstructions of partial derivatives.
- (ii) Compute the singularity indicators according to (3.3).
- (iii) Determine adaptive approximations of the partial derivatives. Using a properly selected threshold δ , define the adaptive approximations of the partial derivatives at the point (x_i, y_j) according to (3.4).
- (iv) Use the third-order TVD Runge-Kutta method for time discretization.

Now, let us consider the difference in the numerical properties between the first-order approximations and the WENO ones from the standpoint of convergence. We denote by φ^n the numerical solution at the *n*th time step and assume that the broken line connecting the points (x_j, φ_j^n) , $j = 0, \pm, \ldots$, is convex (or concave) in the vicinity of the point x_i . Then we get the following estimates with regard to approximations of the derivative,

$$(3.5) \varphi_{i,A}^{n,+} \leqslant \varphi_{i,M}^{n,+} = \varphi_{i+1,M}^{n,-} \leqslant \varphi_{i+1,A}^{n,-} (\varphi_{i,A}^{n,+} \geqslant \varphi_{i,M}^{n,+} = \varphi_{i+1,M}^{n,-} \geqslant \varphi_{i+1,A}^{n,-}).$$

As we can see, the equality $\varphi_{i,M}^{n,+} = \varphi_{i+1,M}^{n,-}$ holds for the first-order approximations but, in general, the inequality $\varphi_{i,A}^{n,+} < \varphi_{i+1,A}^{n,-}$ ($\varphi_{i,A}^{n,+} > \varphi_{i+1,A}^{n,-}$) holds for the WENO approximations. Such difference between two approximations of the derivative directly induces the difference in convergence between the two schemes.

Now, we take a model problem with the Hamiltonian and the initial function defined by

$$H(v) = \begin{cases} 1, & |v| \ge r, \\ 1 + \cos(\pi v/(2r)), & -r < v < r, \end{cases} \quad \varphi_0(x) = \begin{cases} x, & x \le 0, \\ -x, & x > 0, \end{cases} \quad 0 < r < \frac{1}{2}.$$

For the uniform mesh where the cell $[x_i, x_{i+1}]$ is centered at the origin, the WENO approximations of the derivative of φ_0 satisfy the inequalities

$$\begin{split} \varphi_{j,A}^{0,-} \geqslant \varphi_{j,A}^{0,+} \geqslant \varphi_{i,A}^{0,-} \geqslant \varphi_{i,A}^{0,+} \geqslant \frac{1}{2} & (j < i), \\ \varphi_{j,A}^{0,+} \leqslant \varphi_{j,A}^{0,-} \leqslant \varphi_{i+1,A}^{0,+} \leqslant \varphi_{i+1,A}^{0,-} \leqslant -\frac{1}{2} & (j > i+1). \end{split}$$

Using the Godunov flux, we get

$$\widetilde{H}(\varphi_{j,A}^{0,-},\varphi_{j,A}^{0,+}) = \max_{[\varphi_{j,A}^{0,+},\varphi_{j,A}^{0,-}]} H(v) = 1 \quad \forall j.$$

The repeated course according to the time stage shows that the numerical solution converges to the function $\varphi_0(x) - t$. On the other hand, the viscosity solution of the problem has two singular points. (New singularity develops from the origin as the time elapses.) Thus, the WENO scheme fails to converge. As we could know from WENO reconstructions, the WENO scheme cannot take account of the advent of a new singularity caused by the convexity change of the Hamiltonian in this local Riemann problem as the time elapses.

The situation is different from the above for the case of the first-order monotone scheme. In fact, the first-order approximations of the derivative of φ_0 are given by

$$\varphi_{j,M}^{0,\pm} = \varphi_{i,M}^{0,-} = 1 \ (j < i), \quad \varphi_{i,M}^{0,+} = \varphi_{i+1,M}^{0,-} = 0, \quad \varphi_{i+1,M}^{0,+} = \varphi_{j,M}^{0,\pm} = -1 \ (j > i+1).$$

Then we get

$$\begin{split} \widetilde{H}(\varphi_{i,M}^{0,-},\varphi_{i,M}^{0,+}) &= \max_{[0,1]} H(v) = 2, \quad \widetilde{H}(\varphi_{i+1,M}^{0,-},\varphi_{i+1,M}^{0,+}) = \max_{[-1,0]} H(v) = 2, \\ \widetilde{H}(\varphi_{j,M}^{0,-},\varphi_{j,M}^{0,+}) &= 1, \quad j \neq i. \end{split}$$

Therefore, differently from the WENO scheme, the first-order monotone scheme is able to capture the new singularity originating from the initial function as the time elapses.

We notice here that the equality $\varphi_{i,M}^{n,+} = \varphi_{i+1,M}^{n,-}$ for the first-order approximation is turned to the equality $\varphi_{x,i}^{n,+} = \varphi_{x,i+1}^{n,-}$ for the adaptive WENO scheme by Algorithm 1 (when it is estimated that the solution is rough in (x_i, x_{i+1})), which may offer the adaptive WENO scheme a possibility of the convergence.

The following convergence result holds for the adaptive WENO scheme.

Theorem 3.1. For the viscosity solution φ of (2.1) and the solution φ^n of the adaptive WENO scheme by Algorithm 1, the inequality

$$(3.6) |\varphi_i^n - \varphi(x_i, t_n)| \leq C\sqrt{h}, \quad i \in \mathbb{Z}, \quad n = 1, \dots, N,$$

holds, where the constant C depends on φ_0 , H, T and φ .

Proof. For simplicity, we restrict to the case in which the first-order Euler approximation is used for the time derivative. The first-order monotone scheme and the adaptive WENO scheme are rewritten as

$$(3.7) v_i^{n+1} = S^M(v^n)_i, v_i^0 = \varphi_0(x_i), i \in \mathbb{Z}, n = 0, \dots, N-1,$$

(3.8)
$$\varphi_i^{n+1} = S^A(\varphi^n)_i, \quad \varphi_i^0 = \varphi_0(x_i), \quad i \in \mathbb{Z}, \ n = 0, \dots, N-1.$$

As we know ([6]), the monotone scheme (3.7) converges and then the inequality

(3.9)
$$\max_{i} |v_i^n - \varphi(x_i, t_n)| \leqslant C\sqrt{h}, \quad n = 1, \dots, N,$$

holds, where the constant C depends on φ_0 , H, T and φ .

Therefore, we may prove the convergence of the adaptive scheme by estimating the difference between both the solutions of the schemes (3.7) and (3.8). From the monotonicity of the scheme (3.7), we get

$$(3.10) \quad \varphi_{i}^{n+1} - v_{i}^{n+1} = S^{A}(\varphi^{n})_{i} - S^{M}(v^{n})_{i}$$

$$= S^{A}(\varphi^{n})_{i} - S^{M}(\varphi^{n})_{i} + S^{M}(\varphi^{n})_{i} - S^{M}(v^{n})_{i}$$

$$\leq S^{A}(\varphi^{n})_{i} - S^{M}(\varphi^{n})_{i} + S^{M}(\|\varphi^{n} - v^{n}\|_{\infty} + v^{n})_{i} - S^{M}(v^{n})_{i}$$

$$\leq S^{A}(\varphi^{n})_{i} - S^{M}(\varphi^{n})_{i} + \|\varphi^{n} - v^{n}\|_{\infty}.$$

Similarly, we get

(3.11)
$$\varphi_i^{n+1} - v_i^{n+1} \geqslant S^A(\varphi^n)_i - S^M(\varphi^n)_i - \|\varphi^n - v^n\|_{\infty}.$$

On the other hand, from the adaptive WENO approximations (3.2), it holds that

$$(3.12) |\varphi_{x,i}^{n,\pm} - \varphi_{i,M}^{n,\pm}| \leqslant Ch, \quad i \in \mathbb{Z}, \quad n = 0, 1, \dots, N,$$

where the constant C is estimated by L_{∞} -norm of the second order derivative of the solution. In fact, if the numerical solution is smooth in the interval

 $(x_{i-1},x_i)((x_i,x_{i+1}))$, then $\varphi_{i,A}^{n,-}(\varphi_{i,A}^{n,+})$ has still high (at least second) order accuracy (the large six-point stencil may be inoperative in WENO reconstruction). In this case, $\beta_0^-(\beta_0^+) = O(h^2) < \delta$ (= O(h)) and thus $\varphi_{x,i}^{n,\pm} = (\varphi_{x,A}^{n,\pm})$ from (3.2). Therefore, the inequality (3.12) holds true. In other case, we have $\varphi_{x,i}^{n,\pm} = (\varphi_{x,M}^{n,\pm})$ and (3.12) is also true.

From (3.12) and Lipschitz continuity of the numerical Hamiltonian, we get

$$(3.13) |S^{A}(\varphi^{n})_{i} - S^{M}(\varphi^{n})_{i}| = |\widetilde{H}(\varphi_{x,i}^{n,-}, \varphi_{x,i}^{n,+}) - \widetilde{H}(\varphi_{i,M}^{n,-}, \varphi_{i,M}^{n,+})|\Delta t \leqslant C\Delta th.$$

Therefore, we obtain from (3.10), (3.11), and (3.13)

(3.14)
$$\max_{i} |\varphi_{i}^{n+1} - v_{i}^{n+1}| \leq \|\varphi^{n} - v^{n}\|_{\infty} + \max_{i} |S^{A}(\varphi^{n})_{i} - S^{M}(\varphi^{n})_{i}|$$
$$\leq \|\varphi^{n} - v^{n}\|_{\infty} + C\Delta th.$$

By recursion, for $n \leq N$,

(3.15)
$$\max_{i} |\varphi_{i}^{n} - v_{i}^{n}| \leqslant C\Delta t n h \leqslant C h.$$

In the above, we used the same constant C without loss of generality. From (3.9) and (3.15), the desired result follows.

4. Numerical tests

In this section, we illustrate the performance of the proposed schemes in one and two dimensional cases. Below, we denote the WENO scheme in [26] by WENO-ZQ, the WENO scheme proposed in Section 2 by WENO-K and the adaptive WENO scheme by AWENO-K, respectively. The parameters selected are $\nu_1 = 0.998$, $\nu_2 = \nu_3 = 0.001$ in WENO-ZQ and ν_1 may be differently selected in WENO-K according to the problem. The Lax-Friedrichs flux is used in all cases.

 $E \times a \times p \cdot l = 4.1$. We solve the linear equation

(4.1)
$$\begin{cases} \varphi_t + \varphi_x = 0, & -1 < x < 1, \\ \varphi(x, 0) = \sin^9(\pi x) \end{cases}$$

with a periodic boundary condition. Table 1 shows the numerical results by WENO-ZQ and WENO-K at t=2 (CFL = 0.02).

\overline{N}	L^1 error	Order	L^{∞} error	Order	L^1 error	Order	L^{∞} error	Order
		WENO-	ZQ	WENO-K ($\nu_1 = 0.998$)				
40	0.0297		0.1072		0.0260		0.0944	
80	0.0017	4.13	0.0086	3.64	0.0012	4.44	0.0039	4.60
160	3.65e - 5	5.54	1.78e - 4	5.59	2.61e - 5	5.53	8.63e - 5	5.50
320	7.99e - 7	5.51	2.64e - 6	6.07	8.08e - 7	5.01	2.63e - 6	5.03
640	2.53e - 8	4.98	8.29e - 8	4.99	2.53e - 8	4.99	8.29e - 8	4.99
WENO-K ($\nu_1 = 4$)					WENO-K ($\nu_1 = 10$)			
40	0.0204		0.0719		0.0190		0.0630	
80	9.13e - 4	4.48	0.0029	4.63	8.45e - 4	4.49	0.0025	4.66
160	2.58e - 5	5.15	8.31e - 5	5.12	2.58e - 5	5.03	8.30e - 5	4.91
320	8.09e - 7	4.99	2.63e - 6	4.98	8.09e - 7	4.99	2.63e - 6	4.98
640	2.53e - 8	5.00	8.29e - 8	4.99	2.53e - 8	5.00	8.29e - 8	4.99

Table 1. L^1 and L^{∞} errors for Example 4.1, t=2.

Here N denotes the number of grid points of the domain. The errors between the numerical solution and the exact one are estimated by discrete L^1 and L^{∞} -norms defined as

(4.2)
$$\|\varphi^{n} - \varphi(x, t_{n})\|_{1} = \frac{1}{N+1} \sum_{i=0}^{N} |\varphi_{i}^{n} - \varphi(x_{i}, t_{n})|,$$
$$\|\varphi^{n} - \varphi(x, t_{n})\|_{\infty} = \max_{i=0,\dots,N} |\varphi_{i}^{n} - \varphi(x_{i}, t_{n})|.$$

As we can see, the numerical results by the two schemes are comparable with each other and especially, the results by WENO-K are not highly dependent on the selection of parameters according to the gradual refinement of grid.

Example 4.2. We solve the following linear equation

(4.3)
$$\begin{cases} \varphi_t + \varphi_x = 0, \\ \varphi(x, 0) = \varphi_0(x - 0.5), \end{cases}$$

where φ_0 is a periodic function defined as

$$\varphi_0(x) = -\left(\frac{\sqrt{3}}{2} + \frac{9}{2} + \frac{2\pi}{3}\right)(x+1) + \begin{cases} 2\cos\left(\frac{3\pi x^2}{2}\right) - \sqrt{3}, & -1 \leqslant x \leqslant -\frac{1}{3}, \\ \frac{3}{2} + 3\cos(2\pi x), & -\frac{1}{3} \leqslant x < 0, \\ \frac{15}{2} - 3\cos(2\pi x), & 0 \leqslant x < \frac{1}{3}, \\ \frac{28 + 4\pi + \cos(3\pi x)}{3} + 6\pi x(x-1), & \frac{1}{3} \leqslant x < 1. \end{cases}$$

As one knows, the solution of (4.3) is given as $\varphi(x,t) = \varphi_0(x-t-0.5)$. Fig. 1 shows the performance of WENO-ZQ with $\nu_1 = 0.998, \nu_2 = \nu_3 = 0.001$ and $\nu_1 = \nu_2 = \nu_3 = \frac{1}{3}$ at t = 2, 10 (N = 100, CFL = 0.1).

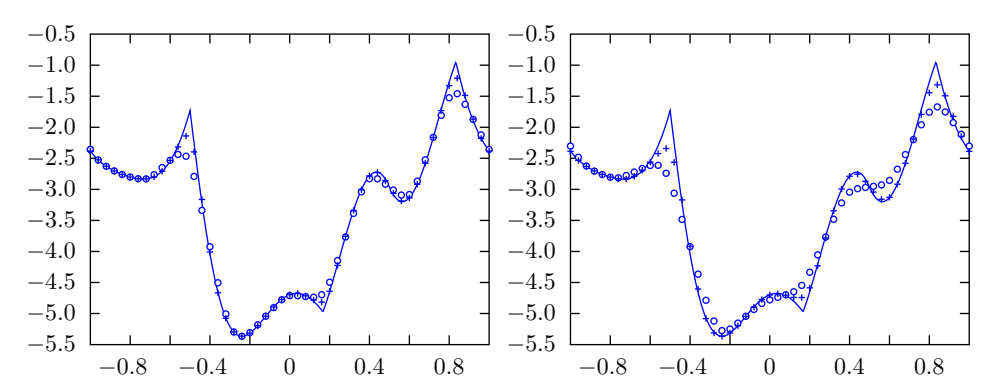


Figure 1. Comparison of WENO-ZQ with different parameters. Left: t=2, right: t=10, open circle: $\nu_1=\frac{1}{3}$ and plus sign: $\nu_1=0.998$.

We observe that the performance of WENO-ZQ for (4.3) is severely affected by the selection of parameters.

\overline{N}	L^1 error	Order	L^{∞} error	Order	L^1 error	Order	L^{∞} error	Order	
	-	WENO-	ZQ	WENO-K ($\nu_1 = 0.998$)					
40	0.1039		0.8978		0.0987		0.8903		
80	0.0299	1.79	0.5277	0.77	0.0291	1.76	0.5185	0.78	
160	0.0090	1.73	0.3093	0.77	0.0087	1.74	0.3071	0.76	
320	0.0028	1.68	0.1693	0.87	0.0028	1.64	0.1672	0.88	
640	9.39e - 4	1.57	0.0959	0.82	9.40e - 4	1.57	0.0935	0.84	
WENO-K ($\nu_1 = 4$)					WENO-K ($\nu_1 = 10$)				
40	0.0895		0.7374		0.0855		0.6743		
80	0.0246	1.86	0.4159	0.83	0.0241	1.83	0.3886	0.80	
160	0.0073	1.75	0.2418	0.78	0.0071	1.76	0.2269	0.78	
320	0.0026	1.49	0.1467	0.72	0.0022	1.69	0.1261	0.85	
640	8.71e - 4	1.58	0.0863	0.77	6.77e - 4	1.70	0.0734	0.78	

Table 2. Comparison of WENO-ZQ and WENO-K, t = 2.

Table 2 shows the numerical results by WENO-ZQ and WENO-K with different values of ν_1 at t=2. The numerical results by WENO-K with $\nu_1=0.998$ are comparable with WENO-ZQ. On the other hand, as was expected, the results by WENO-K show the evident differences according to the selection of ν_1 .

When the problem has a rough solution with great absolute first and second derivatives like (4.3), it holds in computational practice that $\omega_2^{\pm}(\omega_3^{\pm}) \approx O(1)$ (as a matter of fact, it depends on the spacing size h). Then the influence of the fifth-order approximation in WENO reconstruction is relatively strengthened as the parameter ν_1 is increased, and the numerical results by WENO-K are remarkably improved.

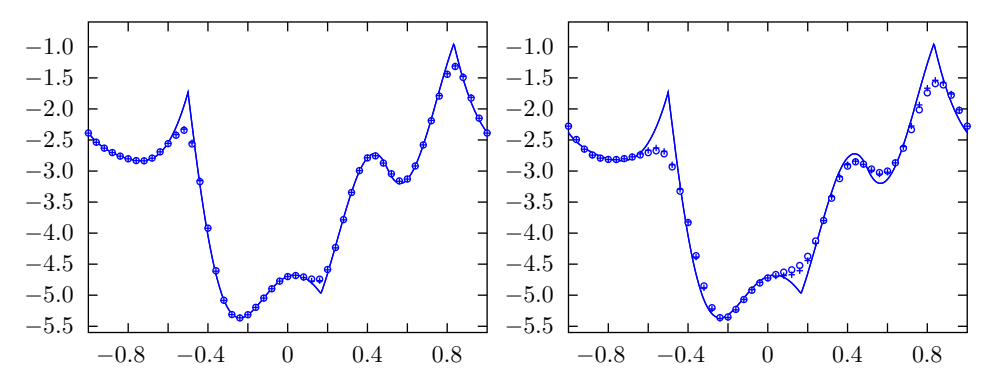


Figure 2. Comparison of WENO-ZQ and WENO-K. Left: t=10, right: t=100, open circle: WENO-ZQ and plus symbol: WENO-K.

Fig. 2 shows numerical results by two schemes with the same parameters ($\nu_1 = 0.998, \nu_2 = \nu_3 = 0.001$) at t = 10,100. The results by the two schemes nearly coincide with each other at t = 10 and the performance of WENO-K is a little superior to WENO-ZQ at t = 100. Fig. 3 shows the numerical results by WENO-ZQ and WENO-K ($\nu_1 = 1, 2, 4, 10, \nu_2 = \nu_3 = 0.001$) at t = 100, t = 500. Here, we refer to WENO-K1, WENO-K2, WENO-K3, and WENO-K4 as $\nu_1 = 1, 2, 4$ and 10, respectively.

The above-mentioned results show the efficiency of WENO-K based on new clear concise nonlinear weights and their convex combination.

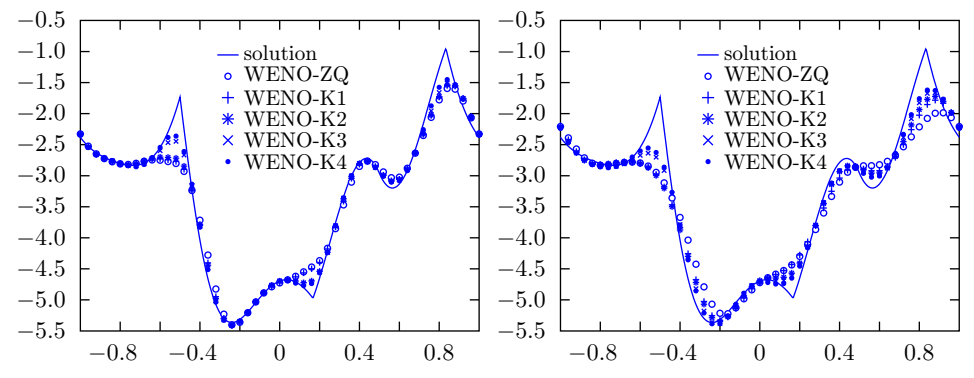


Figure 3. Comparison of WENO-ZQ and WENO-K ($\nu_1=1,2,4,10$). Upper: t=100, lower: t=500.

Example 4.3. Consider the problem

(4.5)
$$\begin{cases} \varphi_t - \cos(\varphi_x + 1) = 0, & -1 < x < 1, \\ \varphi(x, 0) = -\cos(\pi x) \end{cases}$$

with the periodic boundary condition.

\overline{N}	L^1 error	Order	L^{∞} error	Order	L^1 error	Order	L^{∞} error	Order	
		WEN	O-ZQ		WENO-K ($\nu_1 = 1$)				
10	0.0018		0.0035		0.0018		0.0035		
20	2.19e - 4	3.04	6.85e - 4	2.35	2.19e - 4	3.04	6.85e - 4	2.35	
40	1.24e - 5	4.14	1.19e - 4	2.53	1.24e - 5	4.14	1.19e - 4	2.53	
80	$6.56\mathrm{e}-7$	4.24	1.16e - 5	3.56	$6.56\mathrm{e}-7$	4.24	1.16e - 5	3.56	
	WENO-K ($\nu_1 = 4$)					WENO-K ($\nu_1 = 10$)			
10	0.0018		0.0035		0.0018		0.0035		
20	2.05e - 4	3.13	6.84e - 4	2.36	2.02e - 4	3.16	6.83e - 4	2.36	
40	1.24e - 5	4.05	1.19e - 4	2.52	1.24e - 5	4.03	1.19e - 4	2.52	
80	6.56e - 7	4.24	1.16e - 5	3.56	6.56e - 7	4.24	1.16e - 5	3.56	

Table 3. Comparison of WENO-ZQ and WENO-K, $t = 0.5/\pi^2$.

The solution is still smooth at $t=0.5/\pi^2$ and has singularities at $t=1.5/\pi^2$. Table 3 gives L^1 and L^∞ errors for WENO-ZQ and WENO-K at $t=0.5/\pi^2$ (CFL = 0.02). In case that the solution is comparatively gentle as in this example, the numerical results by two schemes almost coincide with each other and moreover, do not depend highly on the selection of parameters. The further numerical results by two schemes with the same parameters at $t=1.5/\pi^2$ also agree with each other.

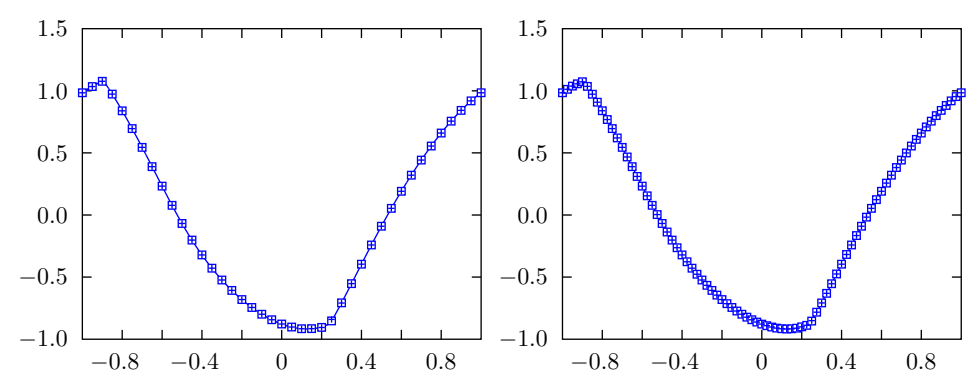


Figure 4. Solid line: reference, square symbol: WENO-K, plus symbol: AWENO-K. Left: $N=40,~\delta=1,$ right: $N=80,~\delta=0.5.$

Fig. 4 shows the performances of WENO-K and AWENO-K at $t=1.5/\pi^2$ ($\nu_1=1$, $\nu_2=\nu_3=0.001$). Here, we used the numerical solution by WENO-JP [10] on the mesh with N=3200 as a reference solution. As we can see through Fig. 4, both the schemes approximate the solution exactly. Especially, the adaptive step by Algorithm 1 with properly selected threshold δ does not affect the accuracy of the final AWENO-K.

Table 4 shows the values of the singularity indicator β_0^+ of the numerical solution of the adaptive WENO scheme with different thresholds at $t = 1.5/\pi^2$ (N = 80). As we can observe from Table 4, the values of the singularity indicator have obvious differences in the neighborhood of singular point.

	Points									
δ	-0.950	-0.925	-0.900	-0.875	0.175	0.200	0.225	0.250	Else points	
0.1	0.109	0.288	1.114	0.194	0.128	0.144	0.407	0.501	less than 0.02	
0.5	0.018	0.018	1.174	0.002	0.008	0.008	1.103	0.143	less than 0.02	
1.0	0.011	0.011	1.145	0.001	0.005	0.005	1.004	0.077	less than 0.02	

Table 4. Singularity indicator β_0^+ of the adaptive approximate solution.

Example 4.4. We solve the problem

(4.6)
$$\begin{cases} \varphi_t + \frac{(\varphi_x + 1)^2}{2} = 0, & -1 < x < 1, \\ \varphi(x, 0) = -\cos(\pi x) \end{cases}$$

with a periodic boundary condition.

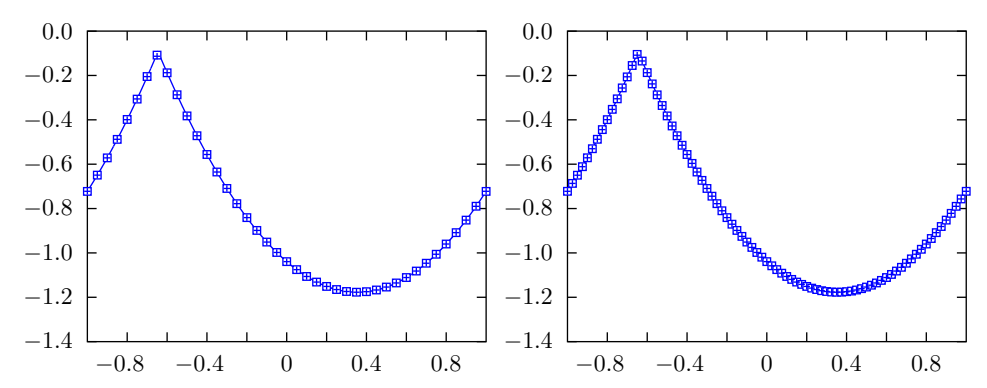


Figure 5. Solid line: reference, square symbol: WENO-K, plus symbol: AWENO-K. Left: $N=40, \ \delta=1, \ {\rm right}: \ N=80, \ \delta=0.5.$

The solution has the singularity (derivative discontinuity) at $t = 3.5/\pi^2$. Fig. 5 shows the numerical results by WENO-K and AWENO-K at $t = 3.5/\pi^2$ ($\nu_1 = 1$,

 $\nu_2 = \nu_3 = 0.001$, CFL = 0.02). The reference solution is obtained by WENO-JP on the mesh with N=3200. Both the schemes also approximate the solution exactly and the numerical results agree with each other. Table 5 shows the values of the singularity indicator β_0^+ of the approximate solution by AWENO-K in comparison with the reference solution at $t=3.5/\pi^2$ (N=80).

	Points								
δ	-0.700	-0.675	-0.650	-0.625	Else points				
0.1	0.020	0.480	1.928	0.009	less than 0.003				
0.5	0.002	0.042	1.124	0.009	less than 0.003				
1.0	0.002	0.010	1.271	0.006	less than 0.003				
Reference	0.0026	0.0026	1.2386	0.0026	less than 0.003				

Table 5. Singularity indicator β_0^+ $(t = 3.5/\pi^2)$.

As Table 5 shows, the values of the singularity indicator have obvious differences in the neighborhood of the singular point.

Example 4.5. We solve the one-dimensional Riemann problem

(4.7)
$$\begin{cases} \varphi_t + \frac{1}{4}(\varphi_x^2 - 1)(\varphi_x^2 - 4) = 0, & -1 < x < 1, \\ \varphi(x, 0) = -2|x|. \end{cases}$$

Fig. 6 shows the results by WENO-K and AWENO-K at t = 1 ($\nu_1 = 1$, $\nu_2 = \nu_3 = 0.001$, CFL = 0.04). The WENO scheme fails to converge for the problem (4.7). Especially, the results by the WENO scheme are unstable with regard to the selection of N. Meanwhile, AWENO-K converges irrespectively of the selection of N. The reference solution is obtained by the first-order monotone scheme on the mesh with N = 500 cells.

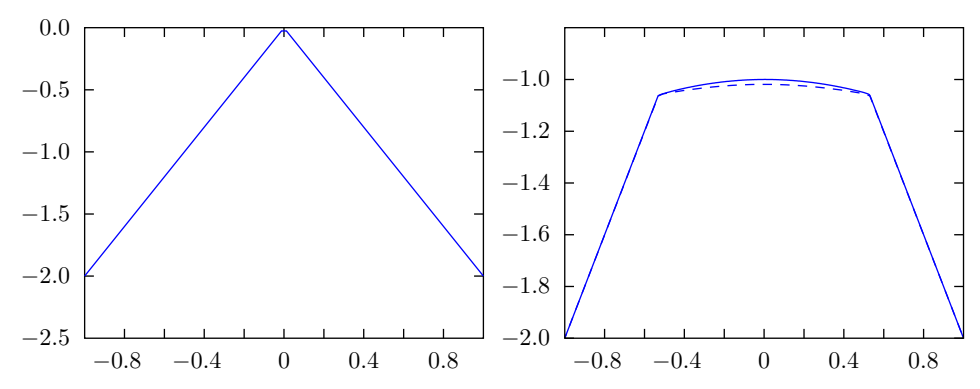


Figure 6. Numerical results for (4.7) (N=81). Left: WENO-K, right: solid line-reference, dotted line: AWENO-K ($\delta=1$).

Example 4.6. We solve the 1D nonconvex problem with the Hamiltonian and the initial function defined by

$$(4.8) \qquad H(v) = \begin{cases} 1, & v < -0.4, \\ \sin(5\pi(v+0.3)) + 2, & -0.4 \leqslant v < 0, \\ -\sin(5\pi(v-0.1)), & 0 \leqslant v < 0.4, \\ 1, & v \geqslant 0.4, \end{cases}$$

$$(4.9) \qquad \varphi(x,0) = \begin{cases} -x - 3, & x \leqslant -3, \\ x + 3, & -3 < x \leqslant -2, \\ -x - 1, & -2 < x \leqslant -1, \\ 2x + 2, & -1 < x \leqslant 0, \end{cases} \qquad \varphi(x,0) = \varphi(-x,0), \quad x > 0.$$

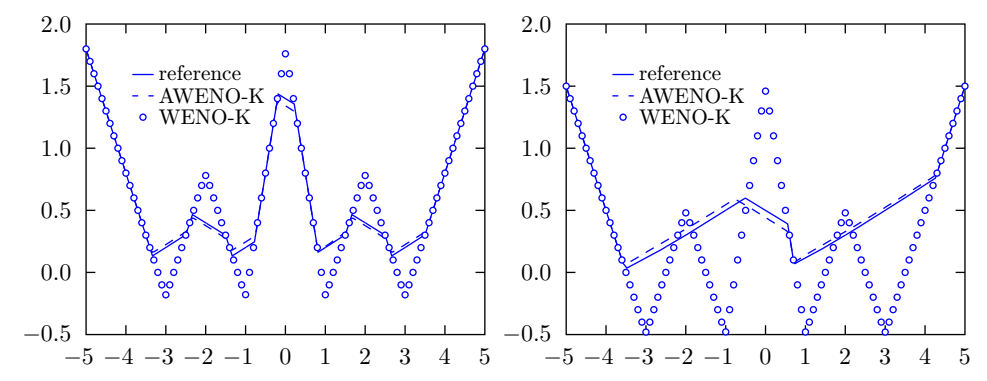


Figure 7. Performances of WENO-K and AWENO-K for Example 4.6. Left: $t=0.2, \, {\rm right}$: t=0.5.

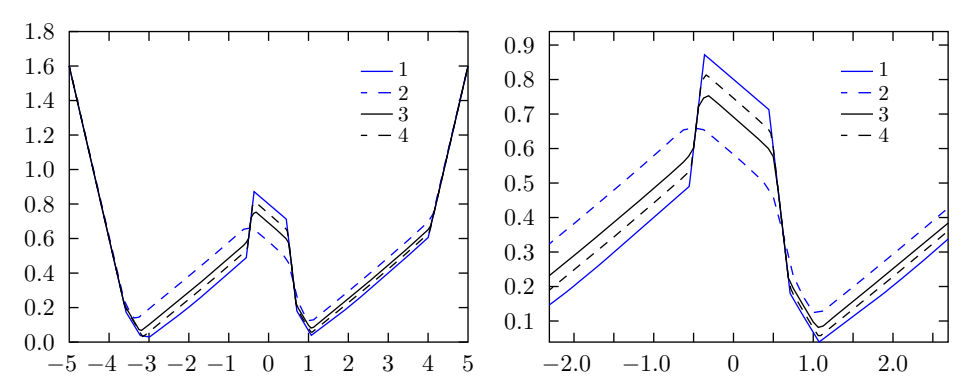


Figure 8. The performance of AWENO-K for Example 4.6 at t=0.4. 1: reference, 2: $N=80,\ 3:\ N=160,\ 4:\ N=320.$

Fig. 7 shows the numerical results by WENO-K and AWENO-K with the mesh N=300 at t=0.2, 0.5 ($\nu_1=1, \nu_2=\nu_3=0.001, \text{CFL}=0.02, \delta=0.01$). More-

over, Fig. 8 shows the performance of AWENO-K according to the different space partitions at t = 0.4. The reference solution is obtained by the Godunov monotone scheme with N=3000 cells. The numerical results verify the convergence of AWENO-K.

Example 4.7. We solve the 2D nonconvex Riemann problem

(4.10)
$$\begin{cases} \varphi_t + \sin(\varphi_x + \varphi_y) = 0, & (x, y) \in [-1, 1] \times [-1, 1], \\ \varphi(x, y, 0) = \pi(|y| - |x|). \end{cases}$$

Fig. 9 shows the performance of AWENO-K for (4.10) at t=1 ($\nu_1=1, \nu_2=1$ $\nu_3 = 0.001, N = 80, \text{ CFL} = 0.1, \delta = 0.5$). The reference solution is obtained by the Godunov monotone scheme with N=320 cells. The contour lines shown in Fig. 9 are comparable with each other.

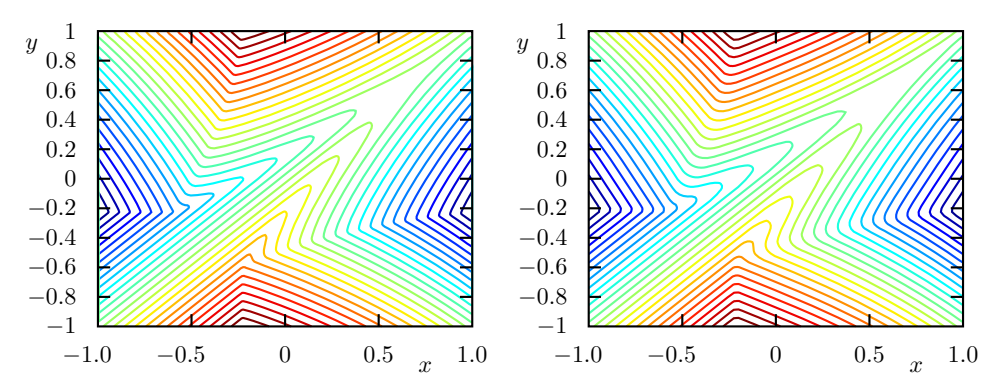


Figure 9. Comparison of contour lines. Left: reference, right: AWENO-K.

Example 4.8. Consider the 2D nonconvex problem

(4.11)
$$\varphi_t + \sin(\varphi_x) + \sin(\varphi_y) = 0, \quad (x, y) \in (-2, 2) \times (-2, 2), \quad t > 0,$$

with the radially symmetric initial condition

with the radially symmetric initial condition
$$(4.12) \qquad \varphi(x,y,0) = \varphi_0(r), \quad r = \sqrt{x^2 + y^2},$$

$$\left\{ \frac{\pi(14r - 13)}{4}, \quad r \leqslant \frac{1}{2}, \right.$$

$$\left\{ \frac{\pi(14r - 13)}{4} + 2\sin(10\pi r), \quad \frac{1}{2} < r \leqslant 1, \right.$$

$$\left\{ \frac{\pi r}{4}, \quad r > 1, \right.$$

and the homogeneous Neumann boundary condition for φ_x and φ_y

(4.13)
$$\begin{cases} \varphi_{xx}(-2, y, t) = \varphi_{xx}(2, y, t) = 0 & \forall y \in [-2, 2], \quad t > 0, \\ \varphi_{yy}(x, -2, t) = \varphi_{yy}(x, 2, t) = 0 & \forall x \in [-2, 2], \quad t > 0. \end{cases}$$

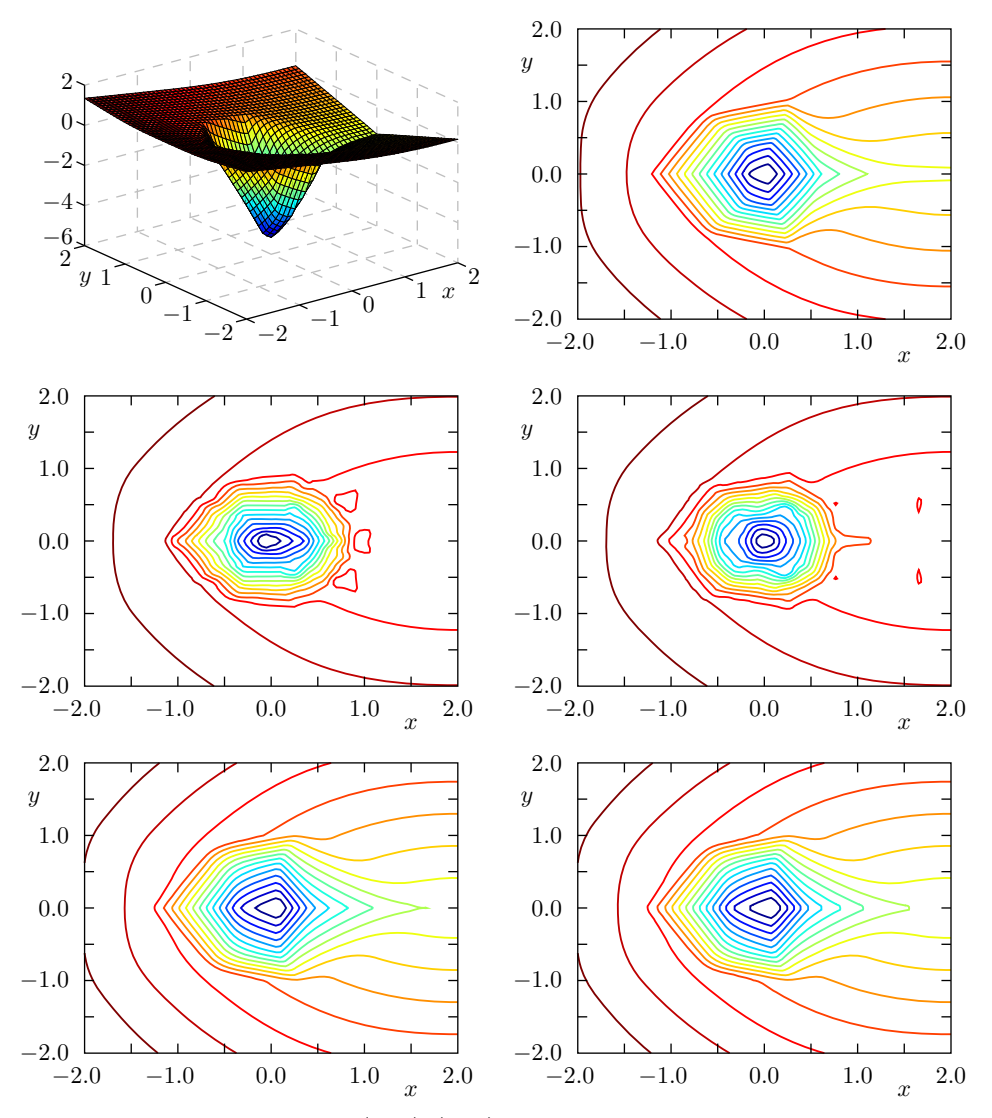


Figure 10. Numerical results for (4.11)–(4.13). Top: reference, middle: WENO-K, bottom: AWENO-K. Left: N=80, right: N=81.

Fig. 10 shows the numerical results by WENO-K and AWENO-K for the equation (4.11)–(4.13) at t=2 ($\nu_1=1,\ \nu_2=\nu_3=0.001,\ {\rm CFL}=0.01,\ \delta=0.1$). The reference solution is obtained by the Godunov monotone scheme on the mesh with N=200 cells. As one can see through the contour lines presented in Fig. 10, the numerical results on meshes with N=80 and N=81 cells exhibit the instability of WENO-K and the numerical solution computed by the pure WENO-K scheme fails to converge to the solution of the problem (4.11)–(4.13). On the other hand,

as compared with the reference solution, we can verify that the numerical solution by AWENO-K converges toward that we believe to be the viscosity solution of the problem (4.11)–(4.13).

Example 4.9. We solve the 2D nonconvex problem

(4.14)
$$\varphi_t + \sin(\varphi_x) + \varphi_y/4 = 0, \quad (x, y) \in (-2, 2) \times (-2, 2), \quad t > 0,$$

with the initial and boundary conditions (4.12) and (4.13).

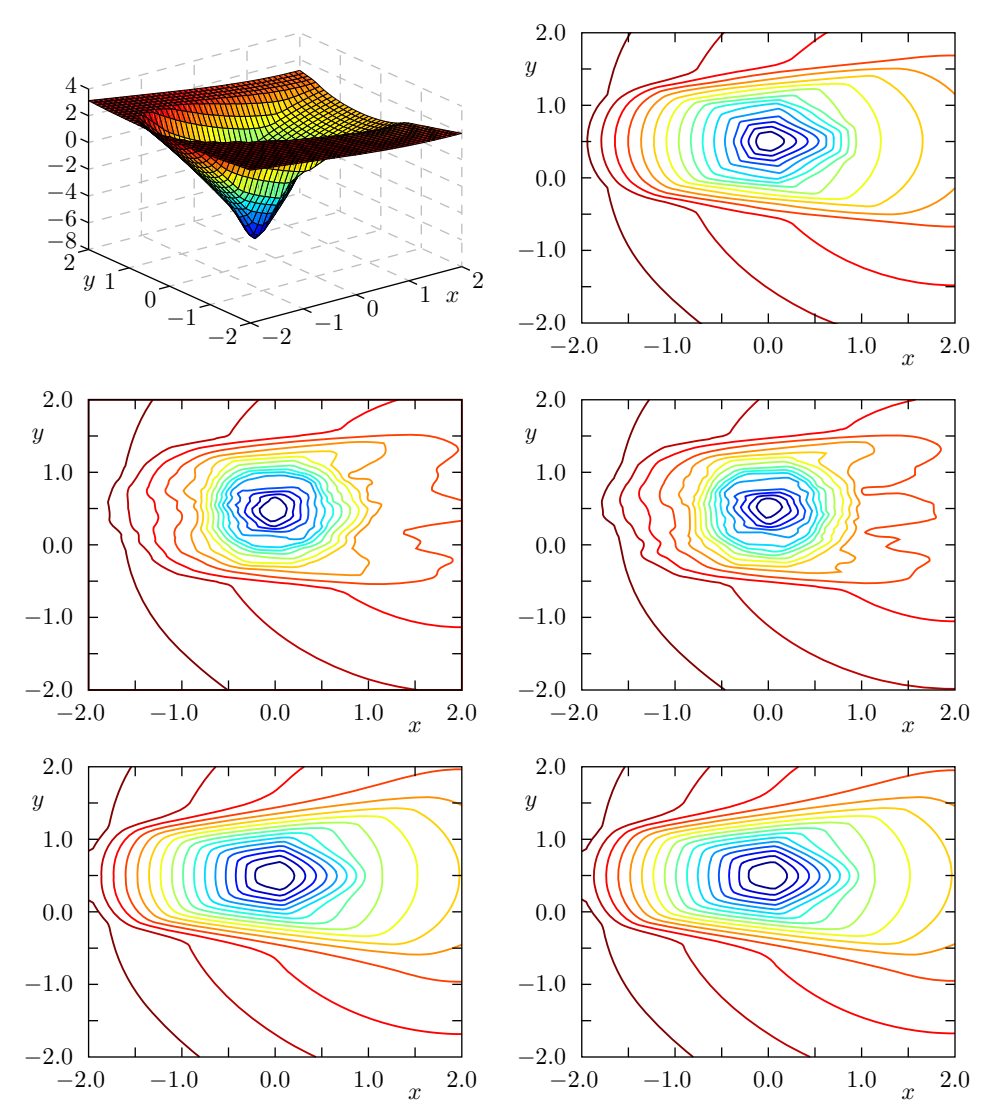


Figure 11. Numerical results for (4.14). Top: reference, middle: WENO-K, bottom: AWENO-K. Left: N=80, right: N=81.

Fig. 11 shows contour lines of numerical solutions computed by both WENO-K and AWENO-K for (4.14) at t=2 ($\nu_1=1$, $\nu_2=\nu_3=0.001$, CFL = 0.01, $\delta=0.1$). The reference solution is obtained by the Godunov monotone scheme with N=320 cells. The numerical results with N=80 and N=81 cells again show the instability of WENO-K as in Example 4.8 and at the same time, we can know that the numerical solution by pure WENO-K fails to converge to the solution of the problem (4.14). As we know in comparison with the reference solution, the numerical solution by AWENO-K converges toward the exact solution of the problem (4.14).

5. Conclusions

In this paper, we have developed WENO schemes of Zhu and Qiu [26] for Hamilton-Jacobi equations by introducing new clear concise nonlinear weights and improving their convex combination. Furthermore, an algorithm of constructing a convergent adaptive WENO scheme has been proposed by applying the simple adaptive step on the proposed WENO scheme, which is based on the introduction of a new singularity indicator. Through detailed numerical experiments on extensive problems including nonconvex ones, the convergence and effectiveness of the adaptive WENO scheme have been demonstrated. Construction of the adaptive WENO scheme on unstructured meshes is the theme of our future study.

References

[1] R. Abgrall: Construction of simple, stable, and convergent high order schemes for steady first order Hamilton-Jacobi equations. SIAM J. Sci. Comput. 31 (2009), 2419–2446. zbl MR doi [2] S. Amat, J. Ruiz, C.-W. Shu: On new strategies to control the accuracy of WENO algorithms close to discontinuities. SIAM J. Numer. Anal. 57 (2019), 1205–1237. zbl MR doi [3] O. Bokanowski, M. Falcone, S. Sahu: An efficient filtered scheme for some first order time-dependent Hamilton-Jacobi equations. SIAM J. Sci. Comput. 38 (2016), A171-A195. zbl MR doi [4] S. Bryson, D. Levy: High-order central WENO schemes for multidimensional Hamilzbl MR doi ton-Jacobi equations. SIAM J. Numer. Anal. 41 (2003), 1339–1369. [5] E. Carlini, R. Ferretti, G. Russo: A weighted essentially nonoscillatory, large time-step scheme for Hamilton-Jacobi equations. SIAM J. Sci. Comput. 27 (2005), 1071–1091. zbl MR doi [6] M. G. Crandall, P.-L. Lions: Two approximations of solutions of Hamilton-Jacobi equations. Math. Comput. 43 (1984), 1–19. zbl MR doi [7] S. Gottlieb, C.-W. Shu, E. Tadmor: Strong stability-preserving high-order time discretization methods. SIAM Rev. 43 (2001), 89–112. zbl MR doi [8] A. K. Henrick, T. D. Aslam, J. M. Powers: Mapped weighted essentially non-oscillarotry schemes: Achieving optimal order near critical points. J. Comput. Phys. 207 (2005), 542 - 567.zbl doi [9] C. Huang: WENO scheme with new smoothness indicator for Hamilton-Jacobi equation. Appl. Math. Comput. 290 (2016), 21–32. zbl MR doi

- [10] G.-S. Jiang, D. Peng: Weighted ENO schemes for Hamilton-Jacobi equations. SIAM J. Sci. Comput. 21 (2000), 2126–2143.
- [11] G.-S. Jiang, C.-W. Shu: Efficient implementation of weighted ENO schemes. J. Comput. Phys. 126 (1996), 202–228.

zbl MR doi

- [12] K. Kim, U. Hong, K. Ri, J. Yu: Construction of convergent adaptive weighted essentially non-oscillatory schemes for Hamilton-Jacobi equations on triangular meshes. Appl. Math., Praha 66 (2021), 599–617.
- [13] K. Kim, Y. Li: Construction of convergent high order schemes for time dependent Hamilton-Jacobi equations. J. Sci. Comput. 65 (2015), 110–137.
- [14] A. Kurganov, G. Petrova: Adaptive central-upwind schemes for Hamilton-Jacobi equations with nonconvex Hamiltonians. J. Sci. Comput. 27 (2006), 323–333.
- [15] D. Levy, S. Nayak, C.-W. Shu, Y.-T. Zhang: Central WENO schemes for Hamilton-Jacobi equations on triangular meshes. SIAM J. Sci. Comput. 28 (2006), 2229–2247. Zbl MR doi
- [16] X.-D. Liu, S. Osher, T. Chan: Weighted essentially non-oscillatory schemes. J. Comput. Phys. 115 (1994), 200–212.
- [17] A. M. Oberman, T. Salvador: Filtered schemes for Hamilton-Jacobi equations: A simple construction of convergent accurate difference schemes. J. Comput. Phys. 284 (2015), 367–388.
- [18] S. Osher, C.-W. Shu: High-order essentially nonoscillatory schemes for Hamilton-Jacobi equations. SIAM J. Numer. Anal. 28 (1991), 907–922.
- [19] J.-M. Qiu, C.-W. Shu: Convergence of high order finite volume weighted essentially nonoscillatory scheme and discontinuous Galerkin method for nonconvex conservation laws. SIAM J. Sci. Comput. 31 (2008), 584–607.
- [20] J.-X. Qiu, C.-W. Shu: Hermite WENO schemes for Hamilton-Jacobi equations. J. Comput. Phys. 204 (2005), 82–99.
- [21] C.-W. Shu: High order weighted essentially nonoscillatory schemes for convection dominated problems. SIAM Rev. 51 (2009), 82–126.
- [22] Z. Xu, C.-W. Shu: Anti-diffusive high order WENO schemes for Hamilton-Jacobi equations. Methods Appl. Anal. 12 (2005), 169–190.
- [23] Y.-T. Zhang, C.-W. Shu: High-order WENO schemes for Hamilton-Jacobi equations on triangular meshes. SIAM J. Sci. Comput. 24 (2003), 1005–1030.
- [24] J. Zhu, J. Qiu: Hermite WENO schemes for Hamilton-Jacobi equations on unstructured meshes. J. Comput. Phys. 254 (2013), 76–92.
- [25] J. Zhu, J. Qiu: A new fifth order finite difference WENO scheme for solving hyperbolic conservation laws. J. Comput. Phys. 318 (2016), 110–121.
- [26] J. Zhu, J. Qiu: A new fifth order finite difference WENO scheme for Hamilton-Jacobi equations. Numer. Methods Partial Differ. Equations 33 (2017), 1095–1113.

Authors' addresses: Wonho Han, Kwangil Kim (corresponding author), Department of Mathematics, University of Sciences, Unjong District 355, 950003 Pyongyang, Democratic People's Republic of Korea, e-mail: kimki1973@star-co.net.kp; Unhyok Hong, Institute of Mathematics, State Academy of Sciences, Unjong District 355, 950003 Pyongyang, Democratic People's Republic of Korea.